

## Hybrid surface waves in twisted anisotropic heterometasurfaces

Xinyan Zhang,<sup>1,2</sup> Chenxu Bian,<sup>1,2</sup> Zheng Gong<sup>1,2</sup>, Ruoxi Chen<sup>1,2</sup>, Tony Low,<sup>3,\*</sup>  
Hongsheng Chen,<sup>1,2,4,5,†</sup> and Xiao Lin<sup>1,2,‡</sup>

<sup>1</sup>*Interdisciplinary Center for Quantum Information, State Key Laboratory of Extreme Photonics and Instrumentation, Zhejiang University, Hangzhou, 310027, China*

<sup>2</sup>*International Joint Innovation Center, The Electromagnetics Academy at Zhejiang University, Zhejiang University, Haining, 314400, China*

<sup>3</sup>*Department of Electrical and Computer Engineering, University of Minnesota, Minneapolis, Minnesota 55455, USA*

<sup>4</sup>*Key Lab. of Advanced Micro/Nano Electronic Devices & Smart Systems of Zhejiang, Jinhua Institute of Zhejiang University, Zhejiang University, Jinhua, 321099, China*

<sup>5</sup>*Shaoxing Institute of Zhejiang University, Zhejiang University, Shaoxing, 312000, China*



(Received 3 January 2024; revised 19 April 2024; accepted 24 May 2024; published 13 June 2024)

Recent advances in twisted photonic structures (e.g., twisted bilayer graphene and twisted anisotropic metasurfaces) have enabled many exotic phenomena of light-matter interactions, such as topological transition of the isofrequency contour of surface waves at the magic angle, photonic flatbands, and localization-to-delocalization transition of light. In general, the optical features of these twisted photonic structures are sensitive to the interlayer twist angle. Here we investigate the mode hybridization of surface waves supported by twisted bilayer anisotropic heterometasurfaces, whose two constituent metasurfaces are nonidentical and support surface waves with similar spatial confinements but distinct polarizations. Counterintuitively, we find that the shape of the isofrequency contour of these hybrid surface waves—eigenmodes with both transverse magnetic and transverse electric wave components—can be insensitive to the twist angle, due to the weak interlayer electromagnetic coupling. Moreover, the interlayer distance provides a unique route to reshape the dispersion of one specific kind of hybrid surface wave, while it has negligible influence on the other kinds. Our finding enriches the physics of light-matter interactions in twisted photonic structures and may open new possibilities to mold the flow of light at the subwavelength scale.

DOI: 10.1103/PhysRevApplied.21.064034

Twisted photonic structures with an interlayer oriented misalignment, such as twisted bilayer graphene [1–9], twisted metasurfaces [10–19], twisted metamaterials [20–25], and twisted photonic crystal slabs [26–30], provide an enticing platform to mold the flow of light both in the far field and in the near field. They have now enabled many exotic phenomena of light-matter interactions [31–35], such as the emergence of photonic flatbands [26,36–39], moiré light lines [40], broadband field canalization [17,25,41,42], localization-to-delocalization transition of light [43–48], and the quantum spin Hall effect of light [49–52].

Twisted bilayer anisotropic metasurfaces are a representative yet complex photonic twisted structure, due to the interplay between the material anisotropy and

their rotational misalignment. When the two constituent metasurfaces are the same, there will be strong near-field electromagnetic coupling between them. Accordingly, the dispersion of surface waves (e.g., metal plasmons, graphene plasmons, and spoof surface plasmons) supported by these twisted bilayer anisotropic homometasurfaces is generally sensitive to the structural geometry, including the twist angle and the interlayer distance. As a typical example, the topological transition of the isofrequency contour of surface waves in twisted  $\alpha$ -phase molybdenum trioxide ( $\alpha\text{-MoO}_3$ ) [22–25] and moiré hyperbolic metasurfaces [17,53–55] will occur at a specific twist angle, namely, the so-called magic angle.

In general, these two constituent metasurfaces are not necessarily the same, and the optical features of surface waves supported by each constituent metasurface, such as their polarizations, can be quite different [56–59]. As background, surface waves supported by an anisotropic metasurface generally have both transverse magnetic (TM) and transverse electric (TE) wave components, and the

\*Corresponding author: tlow@umn.edu

†Corresponding author: hansomchen@zju.edu.cn

‡Corresponding author: xiaolin@zju.edu.cn

polarizations of these hybrid TM-TE surface waves are directly related to the field ratio between their TM and TE wave components. Essentially, this field ratio could vary by orders of magnitude by one merely tailoring the anisotropy of metasurfaces as shown in Figs. 1(b) and 1(c). Looking forward, these twisted bilayer anisotropic heterometasurfaces might provide more opportunities to engineer the dispersion of hybrid surface wave and mold the flow of light at the subwavelength scale. Despite some recent progress regarding twisted van der Waals heterostructures [60–66], the fundamental optical properties of twisted bilayer anisotropic heterometasurfaces are underexplored. Particularly, while the polarization is a fundamental property for these hybrid surface waves, its potential influence on the mode hybridization between the surface waves supported by twisted bilayer anisotropic heterometasurfaces remains elusive.

To address this issue, here we investigate hybrid surface waves supported by twisted bilayer anisotropic heterometasurfaces whose two constituent metasurfaces support surface waves with similar spatial confinements but distinct polarizations. We find that the shape of the

isofrequency contour of these hybrid surface waves can be insensitive to the twist angle, even when the interlayer distance is on the deep-subwavelength scale. This finding indicates that the twisted bilayer anisotropic heterometasurface could have very weak electromagnetic interaction between neighboring nonidentical metasurfaces. Moreover, we reveal that the influence of the interlayer distance on these hybrid surface waves is intrinsically polarization sensitive. To be specific, when the hybrid TM-TE surface waves are dominated by their TM wave component, they are termed “TM-dominant surface waves,” and their dispersion is sensitive to the variation of the interlayer distance. By contrast, when the hybrid TM-TE surface waves have approximately the same strengths of their TM and TE wave components (termed “TM-TE-dominant surface waves”) or are dominated by their TE wave components (termed “TE-dominant surface waves”), their dispersion becomes insensitive to the interlayer distance.

We begin with the introduction of hybrid surface waves supported by a single anisotropic metasurface in Fig. 1(a). Under the coordinate  $xyz$ , the anisotropic metasurface is modeled by a surface conductivity  $\bar{\sigma} = \text{diag}[\sigma_{s,xx}, \sigma_{s,yy}]$ .

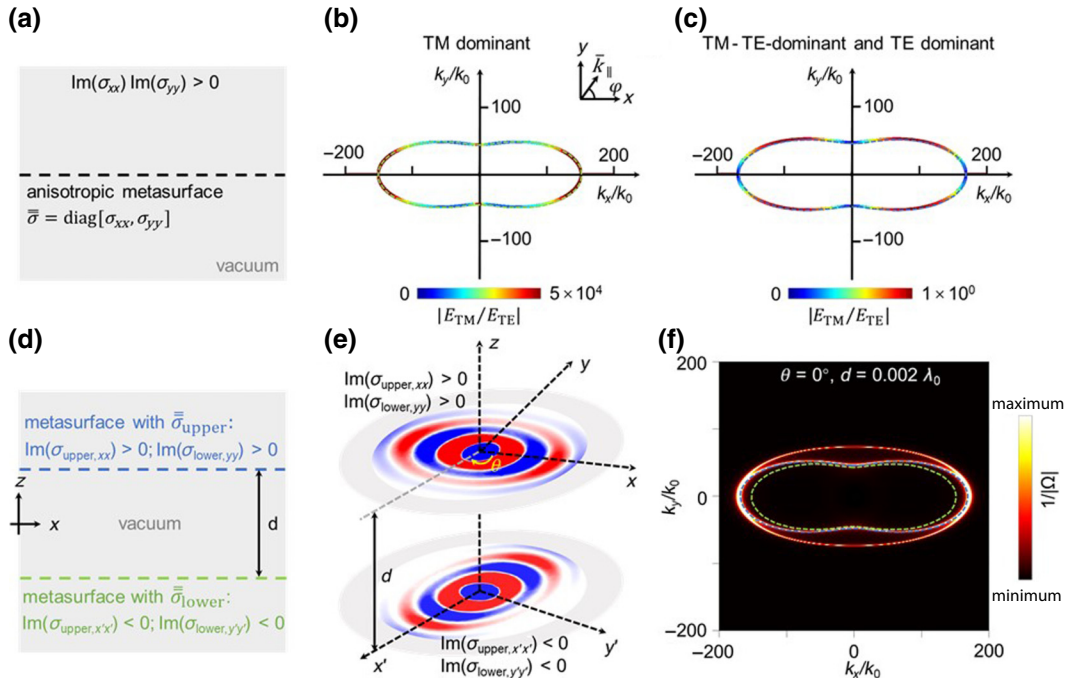


FIG. 1. Hybrid elliptical surface waves supported by twisted bilayer anisotropic heterometasurfaces. The working frequency is chosen to be  $\omega_0/2\pi = 15$  THz, and  $k_0 = \omega_0/c$ . (a) Single metasurface, which supports the propagation of surface waves. (b) Isofrequency contour (represented by a dashed green line) of elliptical TM-dominant surface waves with  $\sigma_{s,xx} = 3.5 \times 10^{-5}i$  S and  $\sigma_{s,yy} = 1.2 \times 10^{-4}i$  S. (c) Isofrequency contour (represented by a dashed blue line) of elliptical TM-TE-dominant and TE-dominant surface waves with  $\sigma_{s,xx} = -0.25i$  S and  $\sigma_{s,yy} = -0.9i$  S. The field ratio between the TM and the TE wave components of hybrid surface waves, namely,  $|E_{TM}/E_{TE}|$ , is shown along the isofrequency contour in (b),(c). In (c), TE-dominant surface waves emerge if  $\bar{k}_{\parallel}$  is almost parallel to  $\hat{x}$  or  $\hat{y}$ , while TM-TE-dominant surface waves emerge if  $\bar{k}_{\parallel}$  is away from  $\hat{x}$  or  $\hat{y}$ . (d),(e) Structural schematic of the designed bilayer heterometasurface produced by directly stacking the two nonidentical anisotropic metasurfaces in (b),(c) together. (f) Isofrequency contour of hybrid surface waves supported by the designed bilayer heterometasurface with twist angle  $\theta = 0^\circ$ . For comparison, the dashed blue and green lines in (b),(c) are also shown in (f). The definition of  $\Omega$  is provided in Eq. (2).

For illustration, this metasurface is placed at the plane of  $z = 0$ , and its surrounding dielectric has relative permittivity  $\varepsilon_r$  (e.g.,  $\varepsilon_r = 1$  used in this work). Below the coordinate transformation is applied for the dispersion calculation. Without loss of generality, the surface waves are assumed to propagate along the  $+\hat{x}'$  direction in a new coordinate  $x'y'z'$  and have a wave vector  $\bar{k} = \hat{z}k_z + \bar{k}_\parallel$ . That is, we have  $\bar{k}_\parallel \parallel \hat{x}'$ , where the azimuthal angle between  $\hat{x}'$  (or  $\bar{k}_\parallel$ ) and  $\hat{x}$  is  $\varphi$  in Fig. 1(b). In this newly established coordinate, the surface conductivity of the metasurface can also be expressed as  $\bar{\sigma}'_s = \begin{bmatrix} \sigma'_{s,xx} & \sigma'_{s,xy} \\ \sigma'_{s,xy} & \sigma'_{s,yy} \end{bmatrix}$ , where  $\sigma'_{s,xx} = \sigma_{s,xx} \cos^2 \varphi + \sigma_{s,yy} \sin^2 \varphi$ ,  $\sigma'_{s,yy} = \sigma_{s,xx} \sin^2 \varphi + \sigma_{s,yy} \cos^2 \varphi$ , and  $\sigma'_{s,xy} = (\sigma_{s,xx} - \sigma_{s,yy}) \sin \varphi \cos \varphi$ . Then by our enforcing the electromagnetic boundary conditions, the dispersion of hybrid surface waves supported by this single metasurface can be obtained as [67]

$$\left(2 + \sigma'_{s,xx} \frac{k_z}{\omega \varepsilon_0 \varepsilon_r}\right) \left(\sigma'_{s,yy} + 2 \frac{k_z}{\omega \mu_0}\right) - \sigma'_{s,xy}^2 \frac{k_z}{\omega \varepsilon_0 \varepsilon_r} = 0, \quad (1)$$

where  $\varepsilon_0$  ( $\mu_0$ ) is the permittivity (permeability) of free space. Generally, the isofrequency contour of hybrid surface waves governed by Eq. (1) is elliptical if  $\text{Im}(\sigma_{s,xx})\text{Im}(\sigma_{s,yy}) > 0$  as shown in Fig. 1, and it will be hyperbolic if  $\text{Im}(\sigma_{s,xx})\text{Im}(\sigma_{s,yy}) < 0$ .

We first consider the hybrid elliptical surface waves supported by an anisotropic metasurface in Fig. 1(a). To characterize the polarization of hybrid surface waves, we show in Figs. 1(b) and 1(c)  $|E_{\text{TM}}/E_{\text{TE}}|$ , namely, the field ratio between the electric field  $E_{\text{TM}}$  of their TM wave component and the electric field  $E_{\text{TE}}$  of their TE wave component, along the trajectory of their isofrequency contour in a  $k_x$ - $k_y$  parameter space.  $|E_{\text{TM}}/E_{\text{TE}}|$  is on the order of  $10^4$  when the metasurface, for example, has  $\sigma_{s,xx} = 3.5 \times 10^{-5}i$  S and  $\sigma_{s,yy} = 1.2 \times 10^{-4}i$  S [Fig. 1(b)]. In other words, the hybrid elliptical surface waves in Fig. 1(b) are dominated by the TM wave component. These TM-dominant surface waves can be further approximately treated as linearly polarized TM surface waves. By contrast,  $|E_{\text{TM}}/E_{\text{TE}}|$  is around 1 if  $\bar{k}_\parallel$  is away from  $\hat{x}$  and  $\hat{y}$  [Fig. 1c], when the metasurface, for example, has

$\sigma_{s,xx} = -0.25i$  S S and  $\sigma_{s,yy} = -0.9i$  S S. These TM-TE-dominant surface waves can no longer be approximately treated as linearly polarized surface waves. In addition, if  $\bar{k}_\parallel$  is very close to  $\hat{x}$  and  $\hat{y}$  [Fig. 1(c)],  $|E_{\text{TM}}/E_{\text{TE}}|$  could be much smaller than 1, and the related surface waves are essentially TE-dominant surface waves. From Figs. 1(b) and 1(c), despite these hybrid TM-dominant, TE-dominant, and TM-TE-dominant surface waves possibly having similar field confinements, their  $|E_{\text{TM}}/E_{\text{TE}}|$  and thus their related polarizations can be quite different. Below we focus the discussion on TM-TE-dominant surface waves, which are under-explored. On the other hand, the anisotropic metasurface with the surface conductivity mentioned can, in principle, be constructed, for example, by structured metal films [68–78] or low-dimensional materials [33,79–88]. Since the hybrid surface waves in Fig. 1 have their in-plane wavelength highly squeezed and are essentially nonradiative, their detection in practice generally relies on some near-field measurement techniques in the microwave regime [89,90] or scattering-type scanning near-field optical microscopy in the infrared regime or the visible regime [22,23].

By our stacking the two nonidentical metasurfaces in Figs. 1(b) and 1(c) together, a twisted bilayer anisotropic heterometasurfaces can be formed. Below, we discuss hybrid surface waves supported by this bilayer heterometasurface as shown in Figs. 1(d) and 1(e). The twisted bilayer anisotropic heterometasurface has twist angle  $\theta$  and interlayer distance  $d$  in Figs. 1(d) and 1(e), where the upper (lower) metasurface is located at the plane of  $z = d/2$  ( $z = -d/2$ ). For twisted photonic structures, the dispersion of surface waves can be calculated with a series of coordinate transformations [23]. For brevity, we refer to the coordinate system aligned with the optical axes of the upper (lower) metasurface as  $xyz$  ( $x'y'z'$ ), and the surface conductivity of the upper (lower) metasurface is denoted as  $\bar{\sigma}_{\text{upper}} = \text{diag}[\sigma_{\text{upper},xx}, \sigma_{\text{upper},yy}]$  ( $\bar{\sigma}_{\text{lower}} = \text{diag}[\sigma_{\text{lower},x'x}, \sigma_{\text{lower},y'y'}]$ ). Meanwhile, we build the  $x''y''z$  coordinate by letting  $\bar{k}_\parallel = \hat{x}''|\bar{k}_\parallel|$ . Correspondingly, the azimuthal angle between  $\bar{k}_\parallel$  and  $\hat{x}$  ( $\hat{x}'$ ) is defined as  $\varphi_1$  ( $\varphi_2$ ). After some calculation, the dispersion of hybrid surface waves supported by this twisted bilayer anisotropic heterometasurface can be obtained as

$$\Omega = \begin{vmatrix} \frac{\sigma_{\text{upper},x''x''} k_z}{\omega \varepsilon_0 \varepsilon_r} e^{ik_z d/2} & -\left(2 + \frac{\sigma_{\text{upper},x''x''} k_z}{\omega \varepsilon_0 \varepsilon_r}\right) e^{-ik_z d/2} & \sigma_{\text{upper},x''y''} e^{ik_z d/2} & \sigma_{\text{upper},x''y''} e^{-ik_z d/2} \\ \frac{\sigma_{\text{upper},x''y''} k_z}{\omega \varepsilon_0 \varepsilon_r} e^{ik_z d/2} & -\frac{\sigma_{\text{upper},x''y''} k_z}{\omega \varepsilon_0 \varepsilon_r} e^{-ik_z d/2} & \sigma_{\text{upper},y''y''} e^{ik_z d/2} & \left(\frac{2k_z}{\omega \mu_0} + \sigma_{\text{upper},y''y''}\right) e^{-ik_z d/2} \\ \left(2 + \frac{\sigma_{\text{lower},x''x''} k_z}{\omega \varepsilon_0 \varepsilon_r}\right) e^{-ik_z d/2} & -\frac{\sigma_{\text{lower},x''x''} k_z}{\omega \varepsilon_0 \varepsilon_r} e^{ik_z d/2} & \sigma_{\text{lower},x''y''} e^{-ik_z d/2} & \sigma_{\text{lower},x''y''} e^{ik_z d/2} \\ \frac{\sigma_{\text{lower},x''y''} k_z}{\omega \varepsilon_0 \varepsilon_r} e^{-ik_z d/2} & -\frac{\sigma_{\text{lower},x''y''} k_z}{\omega \varepsilon_0 \varepsilon_r} e^{ik_z d/2} & \left(\frac{2k_z}{\omega \mu_0} + \sigma_{\text{lower},y''y''}\right) e^{-ik_z d/2} & \sigma_{\text{lower},y''y''} e^{ik_z d/2} \end{vmatrix} = 0, \quad (2)$$

where  $\sigma_{\text{upper},x''x''} = \sigma_{\text{upper},xx} \cos^2 \varphi_1 + \sigma_{\text{upper},yy} \sin^2 \varphi_1$ ,  $\sigma_{\text{upper},y''y''} = \sigma_{\text{upper},xx} \sin^2 \varphi_1 + \sigma_{\text{upper},yy} \cos^2 \varphi_1$ ,  $\sigma_{\text{upper},x''y''} = (\sigma_{\text{upper},xx} - \sigma_{\text{upper},yy}) \sin \varphi_1 \cos \varphi_1$ ,  $\sigma_{\text{lower},x''x''} = \sigma_{\text{lower},xx'} \cos^2 \varphi_2 + \sigma_{\text{lower},yy'} \sin^2 \varphi_2$ ,  $\sigma_{\text{lower},y''y''} = \sigma_{\text{lower},xx'} \sin^2 \varphi_2 + \sigma_{\text{lower},yy'} \cos^2 \varphi_2$ , and  $\sigma_{\text{lower},x''y''} = (\sigma_{\text{lower},xx'} - \sigma_{\text{lower},yy'}) \sin \varphi_2 \cos \varphi_2$ .

According to Eq. (2), Fig. 1(f) shows the isofrequency contour of hybrid surface waves supported by a twisted bilayer anisotropic heterometasurface with twist angle  $\theta = 0^\circ$ . We find that one type of hybrid surface wave in Fig. 1(f) has almost the same isofrequency contour as the TM-TE-dominant surface waves supported by a single metasurface in Fig. 1(c). From this, we can argue that this type of hybrid surface wave is also TM-TE dominant or TE dominant. Actually, the isofrequency contour of these TM-TE-dominant and TE-dominant surface waves supported by the designed bilayer heterometasurface is also insensitive to the interlayer distance. This indicates that the electromagnetic coupling between neighboring

nonidentical metasurfaces is relatively weak, despite the deep-subwavelength interlayer distance. Accordingly, we can infer that the other type of hybrid surface wave in Fig. 1(f) is essentially TM dominant. However, its isofrequency contour in Fig. 1(f) is distinct from the isofrequency contour of TM-dominant surface waves supported by a single metasurface in Fig. 1(b). When the interlayer distance decreases, the isofrequency contour of these TM-dominant surface waves supported by the designed bilayer heterometasurface will expand in the  $k_x$ - $k_y$  parameter space.

We now proceed to discuss the influence of the twist angle  $\theta$  on TM-TE-dominant surface waves supported by this designed heterometasurfaces with a deep-subwavelength interlayer distance as shown in Figs. 2(a)–2(c). Counterintuitively, the primary shapes of these two isofrequency contours remain almost the same for an arbitrary twist angle, apart from their relative angle of orientation. That is, all the TM-dominant,

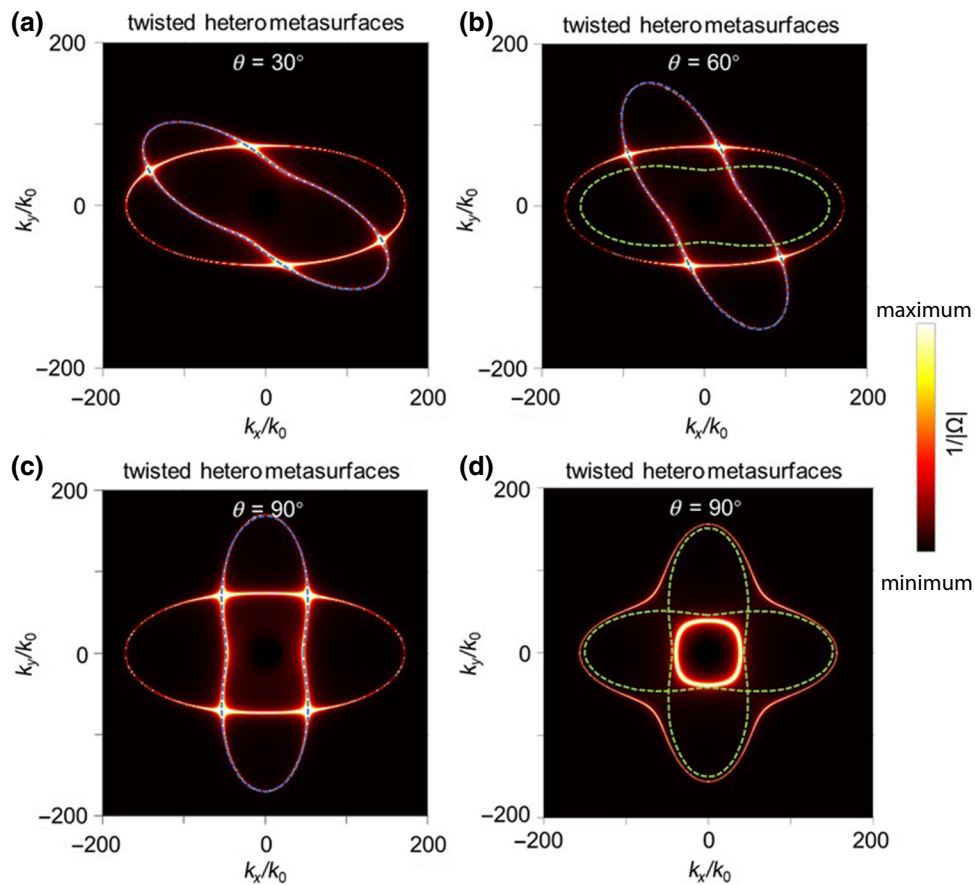


FIG. 2. Influence of the twist angle on hybrid elliptical surface waves supported by twisted bilayer anisotropic heterometasurfaces. (a)–(c) Heterometasurfaces with (a)  $\theta = 30^\circ$ , (b)  $\theta = 60^\circ$ , and (c)  $\theta = 90^\circ$ . The structural setup is the same as in Fig. 1(d), except for the twist angle  $\theta$ . For illustration, the green and/or blue lines from Figs. 1(b) and 1(c) are also shown in (b); meanwhile, the blue line from Fig. 1(c) is rotated by an angle, the same as the twist angle, in each plot. (d) Homometasurfaces, whose lower and upper constituent metasurfaces are both the same as in Fig. 1(b). In (d), one dashed green line is from Fig. 1(b) and the other dashed green line is also from Fig. 1(b) but rotated by  $90^\circ$ . The interlayer distance  $d$  in (a)–(d) is  $0.002\lambda_0$ .

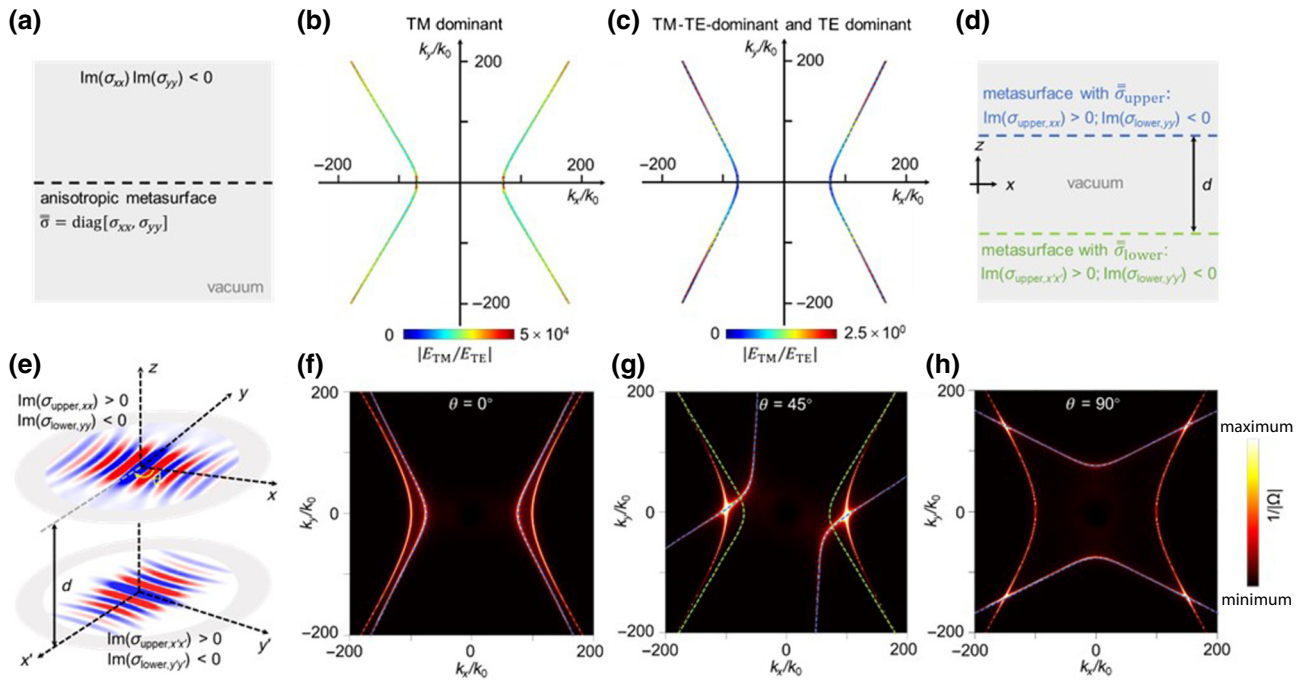


FIG. 3. Hybrid hyperbolic surface waves supported by twisted bilayer anisotropic heterometasurfaces. (a) Single metasurface, which supports the propagation of surface waves. (b) Isofrequency contour (represented by a dashed green line) of hyperbolic TM-dominant surface waves supported by an anisotropic metasurface with  $\sigma_{s,xx} = 7.5 \times 10^{-5}i$  S and  $\sigma_{s,yy} = -2.5 \times 10^{-5}i$  S. (c) Isofrequency contour (represented by a dashed blue line) of hyperbolic TM-TE-dominant and TE-dominant surface waves supported by an anisotropic metasurface with  $\sigma_{s,xx} = 2i$  S and  $\sigma_{s,yy} = -0.4i$  S. In (c), TE-dominant surface waves appear if  $\vec{k}_\parallel$  is almost parallel to  $\hat{x}$ , while TM-TE-dominant surface waves emerge if  $\vec{k}_\parallel$  is away from  $\hat{x}$ . (d),(e) Structural schematic of the designed bilayer heterometasurface produced by our directly stacking the two nonidentical anisotropic metasurfaces in (b),(c) together. (f)–(h) Isofrequency contours of hybrid surface waves supported by the designed heterometasurfaces with twist angle  $\theta$  (whose value is given in each plot) and  $d = 0.002\lambda_0$ . For comparison, the dashed green and blue lines in (b),(c) are also plotted in (g); meanwhile, the blue line from (c) is rotated by an angle, the same as the twist angle, in each plot.

TE-dominant, and TM-TE-dominant surface waves (e.g., their isofrequency contours) supported by the designed twisted bilayer heterometasurfaces may not necessarily be affected by the oriented misalignment between neighboring constituent metasurfaces. By contrast, for the twisted bilayer anisotropic homometasurfaces in Fig. 2(d), the primary shapes of these two isofrequency contours have drastic changes, especially at their crossings. Essentially, these original crossings would disappear, and these two isofrequency contours would merge into one distorted but continuous contour. In this way, the optical feature of twisted bilayer heterometasurfaces in Figs. 2(a)–2(c) is totally distinct from that of twisted bilayer homometasurfaces in Fig. 2(d).

Similarly, the single anisotropic metasurface could also support hyperbolic TM-dominant, TE-dominant, and TM-TE-dominant surface waves when  $\text{Im}(\sigma_{s,xx})\text{Im}(\sigma_{s,yy}) < 0$ . For example, TM-dominant hyperbolic surface waves could emerge when  $\sigma_{1,xx} = 7.5 \times 10^{-5}i$  S and  $\sigma_{1,yy} = -2.5 \times 10^{-5}i$  S as shown in Figs. 3(a) and 3(b), and TM-TE-dominant and TE-dominant hyperbolic hybrid surface waves with a spatial confinement similar to that in Fig. 3(b).

could emerge when  $\sigma_{2,xx} = 2i$  S and  $\sigma_{2,yy} = -0.4i$  S as shown in Fig. 3(c). Below we discuss the hyperbolic TM-dominant, TE-dominant, and TM-TE-dominant surface waves supported by a twisted bilayer anisotropic heterometasurface [Figs. 3(d)–3(h)] produced by our directly stacking the two metasurfaces in Figs. 3(b) and 3(c) together. We find that the exotic phenomenon of hybrid elliptical surface waves revealed in Figs. 1 and 2 can also be extended to hybrid hyperbolic surface waves as shown in Figs. 3(f)–3(h). For example, the isofrequency contours of hyperbolic TM-TE-dominant surface waves in the designed bilayer heterometasurface in Figs. 3(f)–3(h) are the same as the isofrequency contour of TM-TE-dominant surface waves in a single anisotropic metasurface in Fig. 3(c), irrespective to the twist angle and the interlayer distance. The hyperbolic TM-dominant surface waves supported by our designed bilayer heterometasurfaces in Figs. 3(f)–3(h) are insensitive to the twist angle, despite the shape of their isofrequency contour being sensitive to the variation of the interlayer distance.

According to Figs. 3(f)–3(h), the twisted bilayer heterometasurface might offer an enticing platform to mold

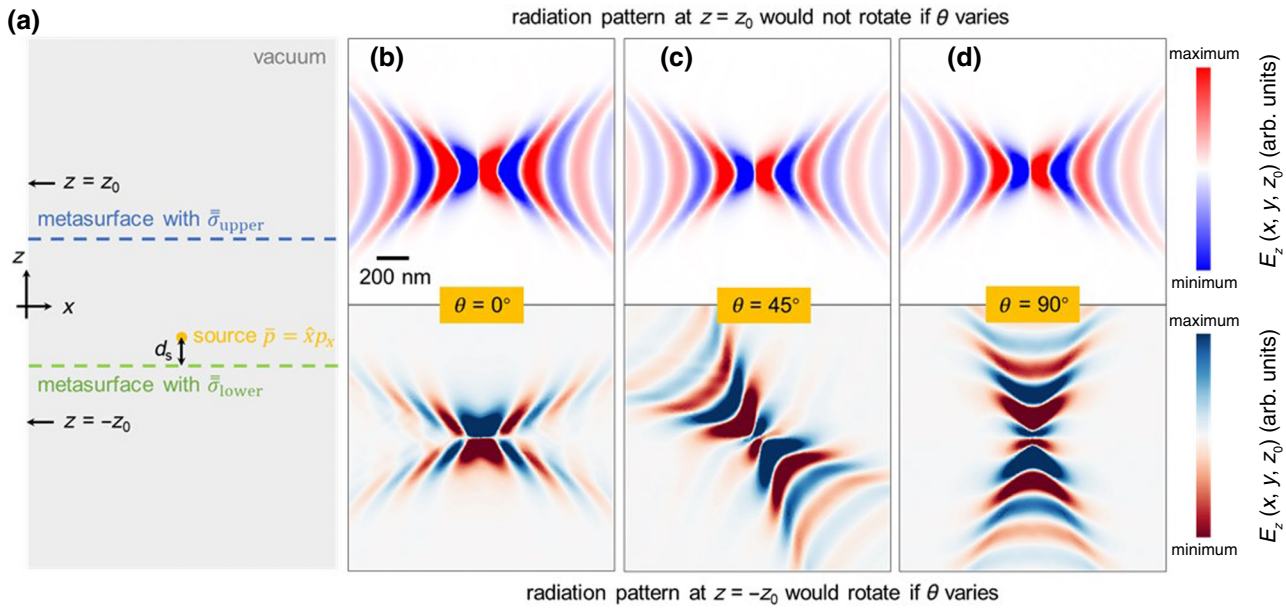


FIG. 4. Molding the flow of light separately in space by exploiting twisted bilayer heterometasurfaces. (a) Structural schematic. The heterometasurfaces here are the same as those in Figs. 3(f)–3(h). The dipolar source has dipole moment  $\bar{p} = \hat{x}p_x$ , and the vertical distance between the source and the lower metasurface  $d_s = 0.0001\lambda_0$ . (b)–(d) Radiation patterns of excited surfaces at  $z = \pm z_0$  for various interlayer twist angles  $\theta$ , where  $z_0 = 0.001\lambda_0$ . For the radiation patterns of the twisted bilayer heterometasurfaces in (b)–(d), the upper metasurface is always fixed, while the lower metasurface is rotated by an angle  $\theta$  with respect to the upper one. Under this scenario, the upper metasurface mainly supports the propagation of TM-dominant surface waves, and accordingly, the radiation pattern of excited surface waves at  $z = +z_0$  will not rotate if  $\theta$  varies. By contrast, the lower metasurface mainly supports the propagation of TM-TE-dominant and TE-dominant surface waves, and the radiation pattern of excited surface waves at  $z = -z_0$  will rotate accordingly if  $\theta$  varies.

the flow of deep-subwavelength surface waves separately in space. For conceptual illustration, a dipolar source with dipole moment  $\bar{p} = \hat{x}p_x$  is placed between the upper and lower metasurfaces [Fig. 4(a)]. As background, all types of surface wave, including TM-dominant, TM-TE-dominant, and TE-dominant surface waves, could be excited by this dipolar source. Under this scenario, the excited surface waves at the plane above the upper metasurface [i.e., the plane of  $z = z_0$  in Fig. 4(a)] essentially correspond to TM-dominant surface waves supported by the upper metasurface, where  $z_0 = 0.001\lambda_0$ . Correspondingly, the radiation pattern of excited surface waves at  $z = z_0$  in Figs. 4(b)–4(d) would not rotate if the twist angle  $\theta$  varies. By contrast, the radiation pattern of excited surface waves at  $z = -z_0$  in Figs. 4(b)–4(d) would rotate accordingly if  $\theta$  varies, since the excited surface waves at  $z = -z_0$  correspond mainly to TM-TE-dominant and TE-dominant surface waves supported by the lower metasurface.

These exotic phenomena of hybrid surface waves revealed in Figs. 1–3 exist widely for twisted bilayer anisotropic heterometasurfaces, as long as their two constituent metasurfaces support hybrid surface waves with similar spatial confinements but distinct polarizations; namely, one constituent metasurface supports TM-dominant surface waves and the other supports

TM-TE-dominant and TE-dominant surface waves. This fact is further verified in Fig. 5, where we let one constituent metasurface support elliptical TM-TE-dominant and TE-dominant surface waves and the other constituent metasurface support hyperbolic TM-dominant surface waves. Under this scenario, only the isofrequency contour of hyperbolic TM-dominant surface waves is sensitive to the interlayer distance. For illustration, we show in Fig. 5 the directional near-field excitation of these TM-dominant surface waves, by placing a point dipolar source close to the designed bilayer heterometasurface. The wavelength of excited TM-dominant surface waves can be readily tuned by changing the interlayer distance [Figs. 5(c)–5(e)] but it is insensitive to the twist angle [Figs. 5(a)–5(c)].

In conclusion, we have investigated hybrid TM-dominant, TE-dominant, and TM-TE-dominant surface waves in twisted bilayer anisotropic heterometasurfaces by letting the two nonidentical constituent metasurfaces support hybrid surface waves with similar spatial confinements but distinct polarizations. We have revealed that all TM-dominant, TE-dominant, and TM-TE-dominant surface waves are robust regarding the variation of the twist angle, despite the interlayer distance being on the deep-subwavelength scale. This exotic feature of hybrid surface waves in twisted heterometasurfaces might

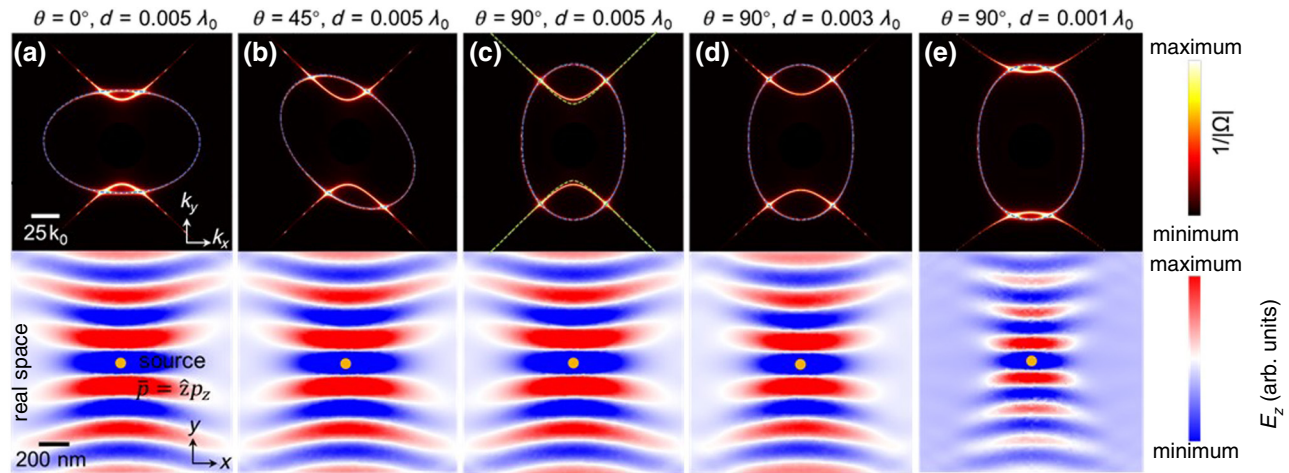


FIG. 5. Hybrid surface waves supported by twisted bilayer anisotropic metasurfaces, whose upper constituent metasurface supports hyperbolic TM-dominant surface waves and whose lower constituent metasurface supports elliptical TM-TE-dominant and TE-dominant surface waves. (a)–(c) Influence of the twist angle. (c)–(e) Influence of the interlayer distance. For illustration, the top panels show the isofrequency contours of hybrid surface waves, and the bottom panels show the distributions of fields [i.e.,  $\text{Re}(E_z)$ ] excited by a dipolar source oscillating parallel to the  $\hat{z}$  direction. The upper constituent metasurface has  $\sigma_{\text{upper},xx} = -7.5 \times 10^{-5} i \text{ S}$  and  $\sigma_{\text{upper},yy} = 7.5 \times 10^{-5} i \text{ S}$  and supports hyperbolic TM-dominant surface waves with an isofrequency contour depicted by the dashed green line in (c). The lower constituent metasurface has  $\sigma_{\text{lower},x'x'} = -0.5 i \text{ S}$  and  $\sigma_{\text{lower},y'y'} = -0.75 i \text{ S}$  and supports elliptical TM-TE-dominant and TE-dominant surface waves with an isofrequency contour depicted by the dashed green line in (a). In addition, the blue line from (a) is rotated by an angle, the same as the twist angle, in each plot.

facilitate the fabrication of some multilayer plasmonic nanostructures, particularly when the interlayer oriented misalignment is not wanted. Moreover, we have found that the interlayer distance could play a crucial role in engineering the dispersion of TM-dominant surface waves, while it has negligible impact on TE-dominant and TM-TE-dominant surface waves. This finding indicates an alternative way to flexibly modulate the propagation of light on the deep-subwavelength scale.

The data that support the findings of this study are available within the article and in Supplemental Material [67].

## ACKNOWLEDGMENTS

X.L. acknowledges support partly from the National Natural Science Fund for Excellent Young Scientists Fund Program (Overseas) of China, the National Natural Science Foundation of China under Grant No. 62175212, the Zhejiang Provincial Natural Science Fund Key Project under Grant No. LZ23F050003, and the Fundamental Research Funds for the Central Universities under Grant No. 226-2024-00022. H.C. acknowledges support from the Key Research and Development Program of the Ministry of Science and Technology under Grants No. 2022YFA1404704, No. 2022YFA1405200, and No. 2022YFA1404902, the National Natural Science Foundation of China under Grant No. 61975176, the Key Research and Development Program of Zhejiang Province under Grant No. 2022C01036, and the Fundamental Research Funds for the Central Universities.

- [1] I. Esin, I. Esterlis, E. Demler, and G. Refael, Generating coherent phonon waves in narrow-band materials: A twisted bilayer graphene phaser, *Phys. Rev. Lett.* **130**, 147001 (2023).
- [2] T. Huang, X. Tu, C. Shen, B. Zheng, J. Wang, H. Wang, K. Khaliji, S. H. Park, Z. Liu, T. Yang, Z. Zhang, L. Shao, X. Li, T. Low, Y. Shi, and X. Wang, Observation of chiral and slow plasmons in twisted bilayer graphene, *Nature* **605**, 63 (2022).
- [3] Y. Wang, G. Yu, M. Rösner, M. I. Katsnelson, H.-Q. Lin, and S. Yuan, Polarization-dependent selection rules and optical spectrum atlas of twisted bilayer graphene quantum dots, *Phys. Rev. X* **12**, 021055 (2022).
- [4] S. Lisi, *et al.*, Observation of flat bands in twisted bilayer graphene, *Nat. Phys.* **17**, 189 (2021).
- [5] X. Zhang, Y. Zhong, T. Low, H. Chen, and X. Lin, Emerging chiral optics from chiral interfaces, *Phys. Rev. B* **103**, 195405 (2021).
- [6] X. Lin, Z. Liu, T. Stauber, G. Gómez-Santos, F. Gao, and H. Chen, Chiral plasmons with twisted atomic bilayers, *Phys. Rev. Lett.* **125**, 077401 (2020).
- [7] E. Y. Andrei and A. H. MacDonald, Graphene bilayers with a twist, *Nat. Mater.* **19**, 1265 (2020).
- [8] A. Nimbalkar and H. Kim, Opportunities and challenges in twisted bilayer graphene: A review, *Nano-Micro Lett.* **12**, 126 (2020).
- [9] S. S. Sunku, G. X. Ni, B. Y. Jiang, H. Yoo, A. Sternbach, A. S. McLeod, T. Stauber, L. Xiong, T. Taniguchi, K. Watanabe, P. Kim, M. M. Fogler, and D. N. Basov, Photonic crystals for nano-light in moiré graphene superlattices, *Science* **362**, 1153 (2018).

- [10] Z. Tan, F. Fan, S. Guan, H. Wang, D. Zhao, Y. Ji, and S. Chang, Terahertz spin-conjugate symmetry breaking for nonreciprocal chirality and one-way transmission based on magneto-optical moiré metasurface, *Adv. Sci.* **10**, 2204 (2023).
- [11] X. Zhang, J. Chen, R. Chen, C. Wang, T. Cai, R. Abdi-Ghaleh, H. Chen, and X. Lin, Perspective on meta-boundaries, *ACS Photonics* **10**, 2102 (2023).
- [12] R. Chen, Z. Gong, J. Chen, X. Zhang, X. Zhu, H. Chen, and X. Lin, Recent advances of transition radiation: fundamentals and applications, *Mater. Today Electron.* **3**, 100025 (2023).
- [13] J. Budhu, E. Michielssen, and A. Grbic, The design of dual band stacked metasurfaces using integral equations, *IEEE Trans. Antennas Propag.* **70**, 4576 (2022).
- [14] C.-W. Qiu, T. Zhang, G. Hu, and Y. Kivshar, Quo vadis, metasurfaces?, *Nano Lett.* **21**, 5461 (2021).
- [15] Q. Zhang, G. Hu, W. Ma, P. Li, A. Krasnok, R. Hillenbrand, A. Alù, and C.-W. Qiu, Interface nano-optics with van der Waals polaritons, *Nature* **597**, 187 (2021).
- [16] Z. Dai, G. Hu, Q. Ou, L. Zhang, F. Xia, F. J. Garcia-Vidal, C.-W. Qiu, and Q. Bao, Artificial metaphotonics born naturally in two dimensions, *Chem. Rev.* **120**, 6197 (2020).
- [17] G. Hu, A. Krasnok, Y. Mazor, C.-W. Qiu, and A. Alù, Moiré hyperbolic metasurfaces, *Nano Lett.* **20**, 3217 (2020).
- [18] M. Renuka, X. Lin, Z. Wang, L. Shen, B. Zheng, H. Wang, and H. Chen, Dispersion engineering of hyperbolic plasmons in bilayer 2D materials, *Opt. Lett.* **43**, 5737 (2018).
- [19] Y. Zhao, M. Belkin, and A. Alù, Twisted optical metamaterials for planarized ultrathin broadband circular polarizers, *Nat. Commun.* **3**, 870 (2012).
- [20] C. Wang, Y. Xie, J. Ma, G. Hu, Q. Xing, S. Huang, C. Song, C. Song, F. Wang, Y. Lei, J. Zhang, L. Mu, T. Zhang, Y. Huang, C.-W. Qiu, Y. Yao, and H. Yan, Twist-angle and thickness-ratio tuning of plasmon polaritons in twisted bilayer van der Waals films, [arXiv:2307.14586](https://arxiv.org/abs/2307.14586).
- [21] J. Chen, X. Lin, M. Chen, T. Low, H. Chen, and S. Dai, A perspective of twisted photonic structures, *Appl. Phys. Lett.* **119**, 240501 (2021).
- [22] G. Hu, Q. Ou, G. Si, Y. Wu, J. Wu, Z. Dai, A. Krasnok, Y. Mazor, Q. Zhang, Q. Bao, C.-W. Qiu, and A. Alù, Topological polaritons and photonic magic angles in twisted  $\alpha\text{-MoO}_3$  bilayers, *Nature* **582**, 209 (2020).
- [23] M. Chen, X. Lin, T. H. Dinh, Z. Zheng, J. Shen, Q. Ma, H. Chen, P. Jarillo-Herrero, and S. Dai, Configurable phonon polaritons in twisted  $\alpha\text{-MoO}_3$ , *Nat. Mater.* **19**, 1307 (2020).
- [24] J. Duan, N. Capote-Robayna, J. Taboada-Gutiérrez, G. Álvarez-Pérez, I. Prieto, J. Martín-Sánchez, A. Y. Nikitin, and P. Alonso-González, Twisted nano-optics: Manipulating light at the nanoscale with twisted phonon polaritonic slabs, *Nano Lett.* **20**, 5323 (2020).
- [25] Z. Zheng, F. Sun, W. Huang, J. Jiang, R. Zhan, Y. Ke, H. Chen, and S. Deng, Phonon polaritons in twisted double-layers of hyperbolic van der Waals crystals, *Nano Lett.* **20**, 5301 (2020).
- [26] H. Qin, Z. Su, M. Liu, Y. Zeng, M.-C. Tang, M. Li, Y. Shi, W. Huang, C.-W. Qiu, and Q. Song, Arbitrarily polarized bound states in the continuum with twisted photonic crystal slabs, *Light: Sci. Appl.* **12**, 66 (2023).
- [27] J. Guan, J. Hu, Y. Wang, M. J. H. Tan, G. C. Schatz, and T. W. Odom, Far-field coupling between moiré photonic lattices, *Nat. Nanotechnol.* **18**, 514 (2023).
- [28] D. X. Nguyen, X. Letartre, E. Drouard, P. Viktorovitch, H. C. Nguyen, and H. S. Nguyen, Magic configurations in moiré superlattice of bilayer photonic crystals: Almost-perfect flatbands and unconventional localization, *Phys. Rev. Res.* **4**, L032031 (2022).
- [29] H. Tang, F. Du, S. Carr, C. De Vault, O. Mello, and E. Mazu, Modeling the optical properties of twisted bilayer photonic crystals, *Light: Sci. Appl.* **10**, 157 (2021).
- [30] K. Dong, T. Zhang, J. Li, Q. Wang, F. Yang, Y. Rho, D. Wang, C. P. Grigoropoulos, J. Wu, and J. Yao, Flat bands in magic-angle bilayer photonic crystals at small twists, *Phys. Rev. Lett.* **126**, 223601 (2021).
- [31] C. Bao, P. Tang, D. Sun, and S. Zhou, Light-induced emergent phenomena in 2D materials and topological materials, *Nat. Rev. Phys.* **4**, 33 (2022).
- [32] L. Liu and Z. Li, Spoof surface plasmons arising from corrugated metal surface to structural dispersion waveguide, *Prog. Electromagn. Res.* **173**, 93 (2022).
- [33] J. Guan, J.-E. Park, S. Deng, M. J. H. Tan, J. Hu, and T. W. Odom, Light-matter interactions in hybrid material metasurfaces, *Chem. Rev.* **122**, 15177 (2022).
- [34] A. Lininger, G. Palermo, A. Guglielmelli, G. Nicoletta, M. Goel, M. Hinczewski, and G. Strangi, Chirality in light-matter interaction, *Adv. Mater.* **34**, 2107325 (2022).
- [35] R. Gutzler, M. Garg, C. R. Ast, K. Kuhnke, and K. Kern, Light-matter interaction at atomic scales, *Nat. Rev. Phys.* **3**, 441 (2021).
- [36] S. A. A. Ghorashi, A. Dunbrack, A. Abouelkomsan, J. Sun, X. Du, and J. Cano, Topological and stacked flat bands in bilayer graphene with a superlattice potential, *Phys. Rev. Lett.* **130**, 196201 (2023).
- [37] S. Tacchi, J. Flores-Farías, D. Petti, F. Brevis, A. Cattoni, A. Cattoni, G. Scaramuzzi, D. Girardi, D. Cortés-Ortuño, R. A. Gallardo, E. Albisetti, G. Carlotti, and P. Landeros, Experimental observation of flat bands in one-dimensional chiral magnonic crystals, *Nano Lett.* **23**, 6776 (2023).
- [38] D. Huang, J. Choi, C.-K. Shih, and X. Li, Excitons in semiconductor moiré superlattices, *Nat. Nanotechnol.* **17**, 227 (2022).
- [39] Z. Zhang, Y. Wang, K. Watanabe, T. Taniguchi, K. Ueno, E. Tutuc, and B. J. LeRoy, Flat bands in twisted bilayer transition metal dichalcogenides, *Nat. Phys.* **16**, 1093 (2020).
- [40] B. Lou, N. Zhao, M. Minkov, C. Guo, M. Orenstein, and S. Fan, Theory for twisted bilayer photonic crystal slabs, *Phys. Rev. Lett.* **126**, 136101 (2021).
- [41] J. Duan, G. Álvarez-Pérez, C. Lanza, K. Voronin, A. I. F. Tresguerres-Mata, N. Capote-Robayna, J. Álvarez-Cuervo, A. Tarazaga Martín-Luengo, J. Martín-Sánchez, V. S. Volkov, A. Y. Nikitin, and P. Alonso-González, Multiple and spectrally robust photonic magic angles in reconfigurable  $\alpha\text{-MoO}_3$  trilayers, *Nat. Mater.* **22**, 867 (2023).
- [42] W. Huang, T. G. Folland, F. Sun, Z. Zheng, N. Xu, Q. Xing, J. Jiang, H. Chen, J. D. Caldwell, H. Yan, and S. Deng, In-plane hyperbolic polariton tuners in terahertz and long-wave infrared regimes, *Nat. Commun.* **14**, 2716 (2023).

- [43] A. A. Arkhipova, Y. V. Kartashov, S. K. Ivanov, S. A. Zhuravitskii, N. N. Skryabin, I. V. Dyakonov, A. A. Kalinkin, S. P. Kulik, V. O. Kompanets, S. V. Chekalin, F. Ye, V. V. Konotop, L. Torner, and V. N. Zadkov, Observation of linear and nonlinear light localization at the edges of moiré arrays, *Phys. Rev. Lett.* **130**, 083801 (2023).
- [44] Z. Meng, L. Wang, W. Han, F. Liu, K. Wen, C. Gao, P. Wang, C. Chin, and J. Zhang, Atomic Bose-Einstein condensate in twisted-bilayer optical lattices, *Nature* **615**, 231 (2023).
- [45] A. Senanian, L. G. Wright, P. F. Wade, H. K. Doyle, and P. L. McMahon, Programmable large-scale simulation of bosonic transport in optical synthetic frequency lattices, *Nat. Phys.* **19**, 1333 (2023).
- [46] P. Wang, Q. Fu, R. Peng, Y. V. Kartashov, L. Torner, V. V. Konotop, and F. Ye, Two-dimensional Thouless pumping of light in photonic moiré lattices, *Nat. Commun.* **13**, 6738 (2022).
- [47] P. Wang, Y. Zheng, X. Chen, C. Huang, Y. V. Kartashov, L. Torner, V. V. Konotop, and F. Ye, Localization and delocalization of light in photonic moiré lattices, *Nature* **577**, 42 (2020).
- [48] Q. Fu, P. Wang, C. Huang, Y. V. Kartashov, L. Torner, V. V. Konotop, and F. Ye, Optical soliton formation controlled by angle twisting in photonic moiré lattices, *Nat. Photonics* **14**, 663 (2020).
- [49] W. Zhang, Y. Wang, D. Xu, and H. Luo, Spin-orbit interaction of light: When twisted light meets twisted metasurfaces, *Phys. Rev. A* **107**, 043502 (2023).
- [50] L. Sheng, X. Zhou, Y. Zhong, X. Zhang, Y. Chen, Z. Zhang, H. Chen, and X. Lin, Exotic photonic spin Hall effect from a chiral interface, *Laser Photonics Rev.* **17**, 2200534 (2022).
- [51] W. J. M. Kort-Kamp, F. J. Culchac, R. B. Capaz, and F. A. Pinheiro, Photonic spin Hall effect in bilayer graphene moiré superlattices, *Phys. Rev. B* **98**, 195431 (2018).
- [52] S. Yuan, J. Yang, Y. Wang, Y. Chen, and X. Zhou, Highly sensitive temperature sensing via photonic spin Hall effect, *Prog. Electromagn. Res.* **177**, 21 (2023).
- [53] S. Yves, E. Galiffi, X. Ni, E. M. Renzi, and A. Alù, Twist-induced hyperbolic shear metasurfaces, [arXiv:2306.01775v1](https://arxiv.org/abs/2306.01775v1).
- [54] S. Liu, S. Ma, R. Shao, L. Zhang, T. Yan, Qi. Ma, S. Zhang, and T. J. Cui, Moiré metasurfaces for dynamic beamforming, *Sci. Adv.* **8**, eab01511 (2022).
- [55] Y. Liu, C. Ouyang, Q. Xu, X. Su, Q. Yang, J. Ma, Y. Li, Z. Tian, J. Gu, L. Liu, J. Han, Y. Shi, and W. Zhang, Moiré-driven electromagnetic responses and magic angles in a sandwiched hyperbolic metasurface, *Photonics Res.* **10**, 2056 (2022).
- [56] X. Zhang, H. Hu, X. Lin, L. Shen, B. Zhang, and H. Chen, Confined transverse-electric graphene plasmons in negative refractive-index systems, *npj 2D Mater. Appl.* **4**, 25 (2020).
- [57] O. Y. Yermakov, A. I. Ovcharenko, A. A. Bogdanov, I. V. Iorsh, K. Y. Bliokh, and Y. S. Kivshar, Spin control of light with hyperbolic metasurfaces, *Phys. Rev. B* **94**, 075446 (2016).
- [58] N. Chamanara and C. Caloz, Graphene transverse electric surface plasmon detection using nonreciprocity modal discrimination, *Phys. Rev. B* **94**, 75413 (2016).
- [59] S. A. Mikhailov and K. Ziegler, New electromagnetic mode in graphene, *Phys. Rev. Lett.* **99**, 016803 (2007).
- [60] X. Guo, W. Lyu, T. Chen, Y. Luo, C. Wu, B. Yang, Z. Sun, F. Javier García de Abajo, X. Yang, and Q. Dai, Polaritons in van der Waals heterostructure, *Adv. Mater.* **35**, 2201 (2023).
- [61] A. T. Costa, M. I. Vasilevskiy, J. Fernández-Rossier, and N. M. R. Peres, Strongly coupled magnon-plasmon polaritons in graphene-two dimensional ferromagnet heterostructures, *Nano Lett.* **23**, 4510 (2023).
- [62] T. Qin, W. Ma, T. Wang, and P. Li, Phonon polaritons in van der Waals polar heterostructures for broadband strong light-matter interactions, *Nanoscale* **15**, 12000 (2023).
- [63] D. J. Rizzo, B. S. Jessen, Z. Sun, F. L. Ruta, J. Zhang, J.-Q. Yan, L. Xian, A. S. McLeod, M. E. Berkowitz, K. Watanabe, T. Taniguchi, S. E. Nagler, D. G. Mandrus, A. Rubio, M. M. Fogler, A. J. Millis, J. C. Hone, C. R. Dean, and D. N. Basov, Charge-transfer plasmon polaritons at graphene/ $\alpha$ -RuCl<sub>3</sub> interfaces, *Nano Lett.* **20**, 8438 (2020).
- [64] F. Hu, M. Kim, Y. Zhang, K. M. Luan, Y. Ho, C. Z. Shi, X. Wang, and Z. Fe, Tailored plasmons in pentacene/graphene heterostructures with interlayer electron transfer, *Nano Lett.* **19**, 6058 (2019).
- [65] T. Low, A. Chaves, J. D. Caldwell, A. Kumar, N. X. Fang, P. Avouris, T. F. Heinz, F. Guinea, L. Martin-Moreno, and F. Koppens, Polaritons in layered two-dimensional materials, *Nat. Mater.* **16**, 182 (2017).
- [66] D. N. Basov, M. M. Fogler, and F. J. Gar, Polaritons in van der Waals materials, *Science* **354**, aag1992 (2016).
- [67] See Supplemental Material at <http://link.aps.org/supplemental/10.1103/PhysRevApplied.21.064034> for calculation of the dispersion of hybrid surface waves supported by a single anisotropic metasurface or a twisted bilayer anisotropic metasurface, and supplemental figures for isofrequency contours and numerical simulations.
- [68] J. Lv, Y. Wu, J. Liu, Y. Gong, G. Si, G. Hu, Q. Zhang, Y. Zhang, J.-X. Tang, M. S. Fuhrer, H. Chen, S. A. Maier, C.-W. Qiu, and Q. Ou, Hyperbolic polaritonic crystals with configurable low-symmetry Bloch modes, *Nat. Commun.* **14**, 3894 (2023).
- [69] F. Ding, A review of multifunctional optical gap-surface plasmon metasurfaces, *Prog. Electromagn. Res.* **174**, 55 (2022).
- [70] D. Yao, P. H. He, H. C. Zhang, J. Zhu, M. Hu, and T.-J. Cui, Miniaturized photonic and microwave integrated circuits based on surface plasmon polaritons, *Prog. Electromagn. Res.* **175**, 105 (2022).
- [71] E. Zhou, Y. Cheng, F. Chen, H. Luo, and X. Li, Low-profile high-gain wideband multi-resonance microstrip-fed slot antenna with anisotropic metasurface, *Prog. Electromagn. Res.* **175**, 91 (2022).
- [72] Q. Chen, Y. Liu, Y. Lei, S. Pian, Z. Wang, and Y. Ma, Recent progress on achromatic metalenses, *Prog. Electromagn. Res.* **173**, 9 (2022).
- [73] S. Chen, W. Liu, Z. Li, H. Cheng, and J. Tian, Metasurface-empowered optical multiplexing and multifunction, *Adv. Mater.* **32**, 1805 (2020).
- [74] W. T. Chen, A. Y. Zhu, and F. Capasso, Flat optics with dispersion-engineered metasurfaces, *Nat. Rev. Mater.* **5**, 604 (2020).

- [75] O. Quevedo-Terue, *et al.*, Roadmap on metasurfaces, *J. Opt.* **21**, 073002 (2019).
- [76] H.-T. Chen, A. J. Taylor, and N. Yu, A review of metasurfaces: Physics and applications, *Rep. Prog. Phys.* **79**, 076401 (2016).
- [77] O. Luukkonen, C. Simovski, G. Granet, G. Goussetis, D. Lioubtchenko, A. V. Räisänen, and S. A. Tretyakov, Simple and accurate analytical model of planar grids and high-impedance surfaces comprising metal strips or patches, *IEEE Trans. Antennas Propag.* **56**, 1624 (2008).
- [78] Y. R. Padooru, A. B. Yakovlev, P.-Y. Chen, and A. Alù, Analytical modeling of conformal mantle cloaks for cylindrical objects using subwavelength printed and slotted arrays, *J. Appl. Phys.* **112**, 034907 (2012).
- [79] M. He, L. Hoogendoorn, S. Dixit, Z. Pan, G. Lu, K. Diaz-Granados, D. Li, and J. D. Caldwell, Guided polaritons along the forbidden direction in MoO<sub>3</sub> with geometrical confinement, *Nano Lett.* **23**, 5035 (2023).
- [80] G. Hu, W. Ma, D. Hu, J. Wu, C. Zheng, K. Liu, X. Zhang, X. Ni, J. Chen, X. Zhang, Q. Dai, J. D. Caldwell, A. Paarmann, A. Alù, P. Li, and C.-W. Qiu, Real-space Nanoimaging of hyperbolic shear polaritons in a monoclinic crystal, *Nat. Nanotechnol.* **18**, 64 (2023).
- [81] X.-R. Wang, X.-B. Wang, H. Ren, N.-S. Wu, J.-W. Wu, W.-M. Su, Y.-L. Han, and X. Su, Optically transparent microwave shielding hybrid film composited by metal mesh and graphene, *Prog. Electromagn. Res.* **170**, 187 (2021).
- [82] H. Hu, X. Lin, and Y. Luo, Free-electron radiation engineering via structured environments, *Prog. Electromagn. Res.* **171**, 75 (2021).
- [83] J. Duan, G. Álvarez-Pérez, K. V. Voronin, I. Prieto, J. Taboada-Gutiérrez, V. S. Volkov, J. Martín-Sánchez, A. Y. Nikitin, and P. Alonso-González, Enabling propagation of anisotropic polaritons along forbidden directions via a topological transition, *Sci. Adv.* **7**, eabf2690 (2021).
- [84] J. Taboada-Gutiérrez, *et al.*, Broad spectral tuning of ultra-low-loss polaritons in a van der Waals crystal by intercalation, *Nat. Mater.* **19**, 964 (2020).
- [85] Z. Zheng, J. Chen, Y. Wang, X. Wang, X. Chen, P. Liu, J. Xu, W. Xie, H. Chen, S. Deng, and N. Xu, Highly confined and tunable hyperbolic phonon polaritons in van der Waals semiconducting transition metal oxides, *Adv. Mater.* **30**, 1705318 (2018).
- [86] F. Xia, H. Wang, D. Xiao, M. Dubey, and A. Ramasubramaniam, Two-dimensional material nanophotonics, *Nat. Photonics* **8**, 899 (2014).
- [87] P. Li, I. Dolado, F. J. Alfaro-Mozaz, F. Casanova, L. E. Hueso, S. Liu, J. H. Edgar, A. Y. Nikitin, S. Vélez, and R. Hillenbrand, Infrared hyperbolic metasurface based on nanostructured van der Waals materials, *Science* **359**, 892 (2018).
- [88] J. S. Gomez-Diaz, M. Tymchenko, and A. Alù, Hyperbolic Plasmons and topological transitions over uniaxial metasurfaces, *Phys. Rev. Lett.* **114**, 233901 (2015).
- [89] F. Gao, Z. Gao, X. Shi, Z. Yang, X. Lin, H. Xu, J. D. Joannopoulos, M. Soljačić, H. Chen, L. Lu, Y. Chong, and B. Zhang, Probing topological protection using a designer surface plasmon structure, *Nat. Commun.* **7**, 11619 (2016).
- [90] C. Qian, X. Lin, Y. Yang, X. Xiong, H. Wang, E. Li, I. Kaminer, B. Zhang, and H. Chen, Experimental Observation of Superscattering, *Phys. Rev. Lett.* **122**, 063901 (2019).